Master's Thesis

Charge Based Detection Platform Using Floating-Gate OFET

Tushar Datta

Student number – 38068

Supervisors - Dr. Fredrik Pettersson,

Prof. Ronald Österbacka

Åbo Akademi

Faculty of Science and Engineering

Physics

Year 2016

Email: tushar.datta@abo.fi

Dedication

I dedicate this work to my parents, Mr. Pravat Chandra Datta & Mrs. Sabita Datta, and my girlfriend Songjukta Chakraborty, for their love and wholehearted support.

Acknowledgements

In autumn of the year 2013, I was first introduced to the Organic Elecronics-group at the Department of Natural Sciences and Physics and Center for Functional Materials (FUNMAT) at Åbo Akademi University by Prof. Ronald Österbacka. Under excellent guidance of Dr. Fredrik Pettersson and Prof. Ronald Österbacka, I completed my laboratory assignment and decided to carry on with my thesis as a part of the Organic Bio-Electronics: Protein Post-translational Modification Sensing using Ion-Modulated OFETs, in short OBESIMO,-project. I am grateful as my thesis was funded by this project and I had a great experience in interdisciplinary learning. I am also thankful to my friend and colleague David Adekanye for his help and advice, laboratory manager Kjell-Mikael Källman for helping me in practical matters and faculty secretary Maisa Tamminen for her help in official processes. Besides all, I am thankful to all my colleagues and mentors of the physics department, for their help and support in daily academic life.

Abstract

The integration of biological molecules to organic semiconducting materials can revolutionize biomedical industry because it has an enormous potential of developing new types of organic bio-electronic devices such as biosensors which are cheaper, more flexible, eco-friendly and bio-compatible. By using solution processable organic (polymer) materials and non-toxic solvents, these devices are not only environmentally friendly, but also R2R-processing compatible and give more flexibility for large area fabrication and design. The electronic properties of biomolecules with the versatility of conductive organic polymers have opened a new era of bio-electronics. Various kinds of organic field-effect transistors (OFETs) have been carefully researched and extensively studied over the last decade and upon development can now compete with silicon technology in terms of performance and quality in some areas. Biosensors belong to this area and with a much better understanding of OFET's, this area can now be explored thoroughly and can produce beneficial results in terms of disposable biosensors for medical care. Here I have tried to develop a 'floating-gate'-enabled OFET-based platform to detect charge based analytes in an aqueous medium, which can subsequently be used to detect protein post-translational modifications (PPTM), which is an important marker for various health-related issues. I have utilized the R2R-compatible aluminum (Al) OFET with chemically anodized aluminum oxide (Al_2O_3) as gate dielectric and the atmospherically stable organic semiconductor poly (3-hexylthiophene) (P3HT) as active layer. The performance of the OFET was further improved by adding an insulating silane self-assembled monolayer (SAM) on top of the ultra-thin Al_2O_3. Using octadecyltrichlorosilane (ODTS) as SAM, this transistor model was able to operate at -4V and had an on/off-ratio on the order of 100 and a sub threshold swing of 130 mV/decade. The completed

precursor platform was able to detect deposited charge to some extent but more thorough analysis and measurements needs to be done in future to clarify the outcomes.

Table of Contents

List of abbreviations & acronyms

Abbreviations	Meaning
AFM	Atomic force microscope
CMOS	Complementary metal-oxide semiconductor
DI	Deionized water
FET	Field-effect transistor
HOMO	Highest occupied molecular orbital
IC	Integrated circuit
IGFET	Insulated gate field-effect transistor
JFET	Junction field-effect transistor
LUMO	Lowest unoccupied molecular orbital
MOSFET	Metal-oxide semiconductor field-effect transistor
OFET	Organic field effect transistor
OLED	Organic light-emitting diode
P3HT	Poly(3-hexylthiophene)
PEDOT:PSS	Poly(3,4-ethylenedioxythiophene) Polystyrene sulfonate
PET	Polyethylene terephthalate
PLLA	Poly(lactic acid) or polylactide (PLA)
PPTM	Protein post-translational modification
PQT-12	Poly(3,3‴-didodecylquaterthiophene)
PVD	Physical vapor deposition
R2R	Roll-t- roll/Reel-to-reel
RFID	Radio frequency identification
SAM	Self-assembled monolayer

List of figures

List of Tables

1. Introduction

The motivation behind the research of organic bio-electronics in general is to combine the versatility of conductive organic polymers and the electronic properties of biological molecules to create more advanced and sophisticated environmentally friendly devices. These can be used in a wide variety of applications, e.g. bio-sensors, bio-actuators, wearable skin patches, electrochemical sensors and so on. In 1948, J. Bardeen and W. H. Brattain in Bell Telephone Laboratories first successfully demonstrated the **trans**fer res**istor** (transistor) operation which revolutionized the modern day electronic circuitry.[1] The invention of transistor technology facilitated tremendous development in the field of electronics. Another significant milestone was the development of the metal-oxide semiconductor field-effect transistor (MOSFET) by Dawon Kahng in the year of 1960 [2] which took integrated circuitry (IC) technology to the next level. FETs are at the heart of all modern day IC devices and the ability to create FETs from organic conductive polymers introduced excellent possibilities for R2R, low cost, disposable electronics. In 1977, Shirakawa, MacDiarmid and Heeger reported on conductivity enhancement in doped poly(acetylene), a ground breaking invention which eventually led to the Nobel prize in Chemistry in the year of 2000.[3] This invention of conductive plastic or polymer changed the way we think about semiconductor technology. The understanding of material properties and utilization of those characteristics helped to develop numerous novel devices using conductive polymers. The maximum resolution, high definition screens available in today's market are built using organic light emitting diodes (OLED). Organic solar cells, radio-frequency identification (RFID) tags and smart windows are a few of the successful products from organic

semiconductor technology. The solution-processability of π-conjugated polymers enabled possibilities of flexible design geometry and low-cost large-scale manufacturing. The growing interest in the area of biomedical applications is due to the bio-compatibility of conductive polymers with bio-systems. Organic bio-electronics is an area with huge potential for conductive polymers.[4]

There are, however, a few challenges with organic electronics, e.g. low voltage-high current application, the efficiency of the device, life time, durability, environmental stability and operation in aqueous media. These challenges need to be resolved in order for applications using the organic polymers/biological molecules-combination can be successful on a larger scale. Working in aqueous media is specifically problematic because it hinders the proper function of the device due to oxidation of the polymer and it also reduces the stability of the device operation. In my work I have investigated a 'floating-gate'-model to separate the sensing platform from the base transistor, which excludes the possibility of damage due to oxidation and ensures proper functioning. The protein post-translational modification (PPTM), phosphorylation is a crucial marker and particularly important in the study of diseases. It plays a pivotal role in the regulation of the cellular environment, thus the development of novel, highly sensitive and sophisticated detection techniques based on phosphorylation is important. Due to changes in the electrical properties of a molecule after any particular PPTM, a charge based detection system can be developed using the organic field-effect transistor (OFET). The electrical change in the solution deposited in a sensing platform gives rise to a capacitive and/or potential difference that can be detected in the adjoining OFET. Due to the unique amplification characteristic of the OFET, this minuscule change can be detected and analyzed afterwards. In this work, my approach is to develop a stable and

environmentally friendly OFET-based charge based detection platform, which uses these properties to detect variation in deposited charges in aqueous media.

2. Theory

2.1 The Field Effect Transistor

Field effect transistors (FETs) are the foundation of modern day circuitries. It is a three-terminal based component where current flows in between the *source*- and *drain* terminals controlled by the bias of the third terminal, known as the *gate*. The conductivity, i.e. the charge carrying capability, of the semiconductor is controlled by an electric field, hence the name field-effect transistor. There are two main types of inorganic FETs: the junction field-effect transistor (JFET) and the metal-oxide semiconductor field-effect transistor (MOSFET). The MOSFET is sometimes called an insulated-gate field effect transistor (IGFET) because its metal-oxide layer works as an insulator layer.[5] The operation principal of JFETs and MOSFETs are different. JFETs are not dependent on metal-oxide-based fabrication techniques.

The thin film transistor (TFT) is made by depositing all its layers on top of each other. Most common TFT example is high quality liquid crystal display (LCD) screens available in today's market. The most similar counterpart of TFT in organic transistors is organic thin film transistors (OTFT). Organic field-effect transistors (OFET) can have same layer structure like TFT/OTFT or it also can adopt a modified structure which is not included in the TFT family.

In this thesis, fabrication is done based on the OFET principle and the experiments are all performed in this specific FET type. However, the transistor calculations of device parameters are based on MOSFET model.

2.2 The MOSFET

MOSFET is basically a charge-controlled device. It is possible to manufacture MOSFETs as enhancement- or depletion-type. For both types, either n-channel (n-MOS) or p-channel (p-MOS) devices can be fabricated. The most popular MOSFETs are enhancement-type devices. Conventional (inorganic) MOSFETs are found in almost all modern electronics. It consists of a conductive substrate which is either negatively (n-type) or positively (p-type) doped, two metallic electrodes (source and drain), a metal-oxide layer and a metal gate. The metal-oxide layer works as an insulating layer to isolate the channel from the metallic gate. Depending on the device type (n or p) three different regions are formed among these layers (i) a pn-junction (ii) a positive/negative doped bulk region in the semiconductor and (iii) an np-junction. Normally the device is in OFF-state, which means that no current is flowing between the source- and drain electrodes, due to the fact that there is no physical penetration of metal through the insulation layer. To turn on the device, or to put it in ON-state, a voltage has to be applied on the gate electrode.

The metallic gate forms a conventional capacitor with the insulator and the semiconductor channel. The gate works as one of the plates of the capacitor; the semiconductor channel works as the second plate and the insulator layer (metal-oxide) works as the dielectric spacer. As in conventional capacitors, when a bias

voltage is applied to one of the plates, an opposite and equal charge will accumulate on the other. E.g. if a large enough negative voltage, is applied to the gate, then the interfacial *hole* density will be large enough to form a p-type channel between the source- and drain electrodes in the semiconductor, through which a current will start to flow. In this case the positive holes are the charge carriers. Since the MOSFET can be manufactured so that the channel carries either *electrons* or *holes*, the MOSFET is said to be a unipolar device.

2.3 Energy Bands

Every kind of material has its own characteristic energy band structure from which its conductivity properties can be studied.

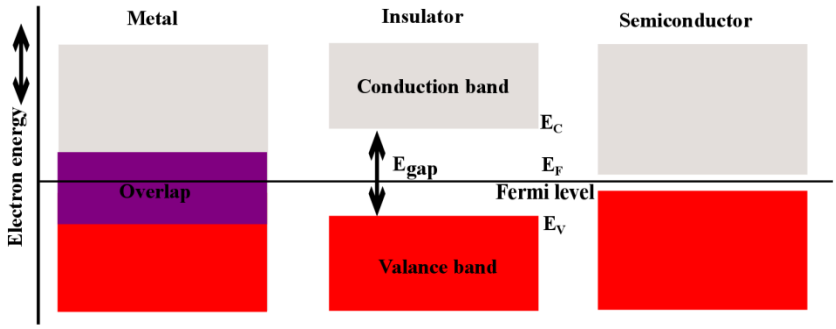

Figure 1. Energy band diagrams of metal, insulator and semiconductor materials, where E_C, E_F and E_V is for conduction band, Fermi level and valance band respectively. Egap shows the 'forbidden gap' between valance band and conduction band of an insulator.

In metal, at $T = 0$ K, the region below the Fermi level, E_F is completely filled with electrons, while the region above E_F is empty. With a small electric field applied, these electrons are free to move into the upper empty region of the conduction band, which results in high conductivity in metals. At $T > 0$ K, electrons have the possibility, due to thermal energy; freely transfer over the Fermi energy level. This is also true for insulator and semiconductor; however, the available holes differ. E.g. in metals the number of holes is larger.

In an insulator, the valance band and the conduction band is separated by a large gap, E_{gap}, a forbidden range of energies. The Fermi level, E_F lies in between these two bands, at midpoint. In insulators, E_{gap}, is typically larger than 4 eV. At $T = 0$ K, the valance band is filled with electrons and the conduction band is completely empty. Even at $T > 0$ K, electrons are usually not thermally excited enough, to travel through this large energy gap, even if an external electric field is applied, thus making insulators non-conductive.

In semiconductors, E_{gap} is typically less than < 2 eV and thus have resistivity in between metals and insulators. E_F is at the midpoint of the E_{gap}. At $T = 0$ K, the valance band is filled with electrons and the conduction band is empty. At $T > 0$ K, electrons are thermally excited and can travel through the small energy gap and partially fill the conduction band and show some conductivity. However, if an external electric field is applied, electrons can easily overcome E_{gap} and become highly conductive.

Intrinsic or ideal semiconductors are pure forms of semiconductors without any impurities or doping. The number of *holes* and *electrons* are equal in intrinsic semiconductors. In higher temperatures or in applied external electric fields when electrons move from valance band to conduction band they leave '*holes*' behind

in their positions. Both the *electrons* and the *holes* can then act as mobile negative- and positive charge carriers, respectively. They are usually represented as *n* and *p*, respectively. For intrinsic semiconductor materials *electrons* and *holes* are always created in pairs and this 'electron-hole pair creation' can be expressed as:

$$n = p = n_{\mathrm{i}} \qquad (2.1)$$

Where n_i stands for 'intrinsic carrier concentration'.

Extrinsic semiconductors are produced by adding controlled impurities or doping. Depending on the donor atom, an extrinsic semiconductor can either be *n*-type or *p*-type.

2.4 The Fermi-Dirac Distribution Function and Fermi Level

In the empty conduction band of semiconductor materials, there are many allowed energy levels available. How electrons will fill these energy levels and will contribute to the conduction depends on a few different factors. The main factors are how many energy levels there are within a given energy range and the probability of an electron to occupy those levels.

The probability for an electron to occupy an energy level can be calculated by a function called the *Fermi-Dirac distribution function, f(E),* where *E* stands for the energy of a specific level. This can be mathematically expressed as:

$$f(E) = \frac{1}{1 + \exp\left(\frac{E - E_{\mathrm{F}}}{k_{\mathrm{B}}T}\right)} \qquad (2.2)$$

Where k_B is Boltzmann's constant, 8.862 x 10^{-5} eV/K and T is the temperature in Kelvin.

$E_{F,}$ shown in Fig. 1 is determined as the energy level, where the probability of finding an electron is 50%. It can be expressed as:

$$f\,(E_{\mathrm{F}}) \;=\; 1/(1 \;+\; \exp((E_{\mathrm{F}} - E_{\mathrm{F}})/(k_{\mathrm{B}}T)) \;=\; 1/(1 \;+\; \exp(0)) \;=\; ½ \qquad (2.3)$$

2.5 The Organic Field Effect Transistor

Organic polymer-based FETs are emerging as an alternative approach for existing Si-based biomedical applications. Because of their mechanical flexibility and enhanced biocompatibility, they are attractive alternatives of conventional inorganic devices. The basic work principal of inorganic MOSFETs and organic FETs (OFETs) are similar in many ways. There are, however, some important differences based in the components and device structures used. The most similar inorganic counterpart to the OFET is TFT. The TFT has a structure where the different layers are deposited on top of one another, on top of a non-conductive substrate.

In general, like conventional MOSFETs and TFTs, OFETs are also three-terminal devices. An OFET is constructed of an organic-semiconductor (π-conjugated polymer), an organic insulator (sometimes metal-oxide) and metallic or organic electrodes.

One of the basic structural differences between OFETs and conventional MOSFETs is that the source- and drain electrodes are in direct contact with the semiconductor material. In an OFET the active material used is usually a π-conjugated semiconductor. The most used OFETs are accumulation- or enhancement-mode devices, where the semiconductor is intrinsic. When the applied gate bias exceeds a specific threshold voltage, a high charge density is formed in the semiconductor, near the insulator interface resulting in the reduction of the resistance between the source- and drain electrodes and a charge (current) starts to flow through this newly formed transistor channel.

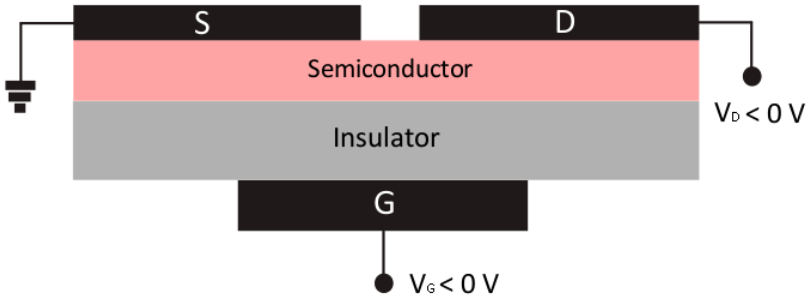

Figure 2. The schematic diagram for a p-channel OFET. The active channel is situated at the semiconductor-insulator interface. With substantial gate bias voltage, conduction starts between source and drain.

The work principal of an OFET is based on a capacitive formed channel in the semiconductor. The physical mechanism for the channel formation is, however, critically different from that of a MOSFET, discussed in section 2.2. To understand the capacitive channel formation in an OFET, we can compare it to a simple metal-insulator-metal parallel plate capacitor, illustrated in Fig. 3.

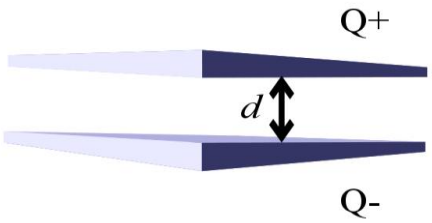

Figure 3. Two metallic plate capacitor formations where Q+ and Q- represents opposite charge and d is the gap between these two plates typically shows the insulator thickness.

Here in an uncharged state, there is no charge on these two metallic plates (conductors). An external potential ΔV is applied to the plates. The amount of charge that is accumulated is proportional to $C*\Delta V$. Mathematically this can be expressed as,

$$Q = C\,|\,\Delta V\,| \qquad (2.4)$$

Where, C is a proportionality constant known as *capacitance*, which has the SI unit of *farad*, F. C can be expressed as,

$$C = \frac{\varepsilon\,\varepsilon_o\,A}{d} \qquad (2.5)$$

Where, ε is the permittivity (dielectric constant) of the material between the plates (for vacuum, $\varepsilon = 1$), ε_0 is the electric constant ($\varepsilon_0 \approx 8.854\times10^{-12}$ F·m^{-1}), A is the area of overlap of the two metallic plates and d is the separation between two plates of the capacitor.

In terms of an OFET, one of these conductors is the gate electrode and the other the conductive channel in the organic semiconductor, at the

semiconductor/insulator-interface. It requires ohmic source and drain electrodes so that charges can be drawn into the channel.

The OFET is fabricated using different deposition techniques in order to form subsequent thin layers. Semiconductor materials are often soluble in organic solvents and can e.g. be processed by drop-coating or spin-coating. Other layers, e.g. the inorganic electrode layers, can be processed by physical vapor deposition, chemical deposition etc. Depending on application and purpose, the thickness of these various layers may vary from a few nanometers to several micrometers. The physical position of the three terminals of the OFET, the source, the drain and the gate, is crucial for proper device operation. The active channel is formed between source and drain electrode at the semiconductor-insulator interface. This active channel is separated by the insulator from the gate electrode. Depending on application four basic OFET structures are available; these are shown in figure 4.

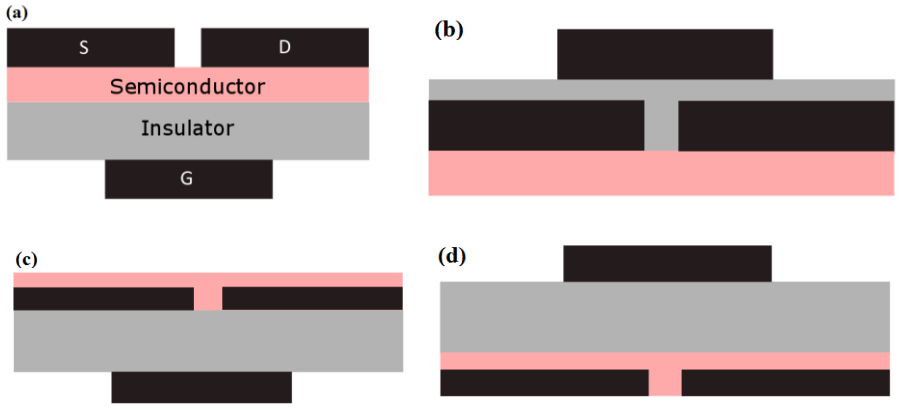

Figure 4. Schematics of the four basic OFET structures. They are (a) the top-contact, bottom-gate- (b) the top-contact, top-gate-, (c) the bottom-contact, bottom-gate- and (d) the bottom-contact, top-gate transistor structures.

Based on the positioning of the three terminals, these are the top-contact bottom-gate-, the top-contact top-gate-, the bottom-contact bottom-gate- and the bottom-contact-, top-gate formations.

An OFET structure should fulfill some criteria in order to achieve the desired device operation. The semiconductor-insulator interface plays a crucial role in device performance. It has a strong influence on contact resistance, active channel formation and capacitance. To avoid stray capacitances or edge effects, it is crucial to align the gate directly underneath, or over, the active channel. In an OFET, the total resistance, *R*, can be measured from three resistances connected in series. These resistances are the contact resistance at the source (R_s) and at the drain (R_D) and the channel resistance (R_{CH}). *Ohmic* source and drain contacts are desired. Total resistance can be expressed as:

$$R = R_{\mathrm{s}} + R_{\mathrm{D}} + R_{\mathrm{CH}} \qquad (2.6)$$

For proper device performance, Eq 2.6 implies that the total contact resistances should be negligible compared to the channel resistance. In OFETs, the channel resistance starts to decrease with increasing V_G when charge carriers start accumulating at the semiconductor-insulator interface. As the layers in an OFET is fabricated in a subsequent manner, the choice of solvent also one of the more important factors to consider. A subsequent layer must not dissolve the underlying layer. Especially the dielectric-semiconductor interface, which plays the principal role in charge transport, must not be allowed to be transformed due to this effect.

The electrical characteristics of OFETs are largely dependent on the device architecture. In TFT devices e.g., a top-contact structure gives a lower contact resistance, mainly due to metal penetration into the semiconductor surface during the evaporation of the source- and drain electrodes, which results in an intermixed

layer.[6] Also, a bottom-gate top-contact structure is geometrically better suited for the floating gate OFET design, which I used in some of the experiments presented in this thesis.

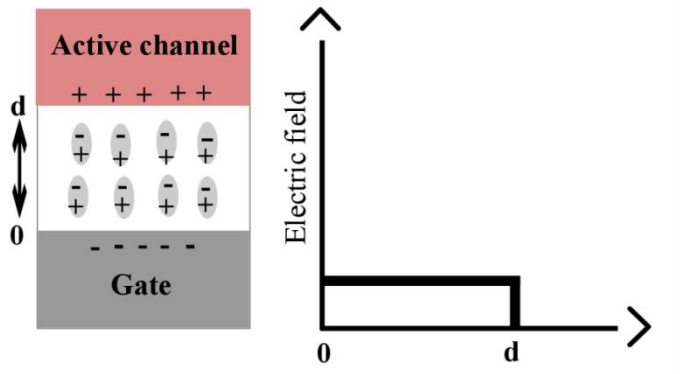

Figure 5. Schematic representation of the charge polarization and electric field distribution in a dielectric gated OFET.

2.6 Charge Transport in Organic Materials

2.6.1 HOMO & LUMO

π-conjugated polymers or materials like ethylene (C_2H_4) which contain π-electrons have special characteristics. Their sp^2 hybridized carbon can form co-planar σ-bonds with other carbon and hydrogen in the chain. The p_z orbital remains perpendicular to the sp^2 hybridized orbital plane which leads to additional π-bonding between two carbon atoms. Thus these molecular orbitals split into bonding and anti-bonding states. Two of these states are of utmost importance, namely the states commonly known as HOMO (highest occupied molecular

orbital) and LUMO (lowest un-occupied molecular orbital). In a neutral, uncharged molecule, the HOMO is the level directly below the narrow energy gap of the semiconductor and the LUMO is the level just above the energy gap. The energy gap is the energy difference between these two states and the energy of HOMO is lower than the LUMO. Electrons tend to minimize their energies and thus always try to occupy the lowest energy state available, either in the HOMO (ground state) or the LUMO (excited). The holes, being the absence of electrons behave conversely and thus tend to reach the highest energy states available. The narrow energy gap between HOMO and LUMO holds electrons and holes in their respective lowest energy states, until any external excitation occurs and then an electron (a hole) can pass through the energy gap into the LUMO (HOMO) and contribute to the electron (hole) conductivity.

When these molecules form solids, they use weak 'Van-der Waal' bonds for intermolecular bonding. Their HOMO and LUMO levels can make narrow energy bands but because of their weak intermolecular bonding the electronic properties of the organic materials are mainly determined by the molecules themselves.

Organic polymers have π-conjugation along their backbone structure and their conductivity can be modulated by several orders of magnitudes by doping. In *p*-type doping it causes depopulation of the bonding π-orbital (HOMO) and results in the formation of holes.

In this work, *p*-type regioregular P3HT was used as organic semiconductor which has 5 eV HOMO and 3 eV LUMO orbital energy. [7,8]

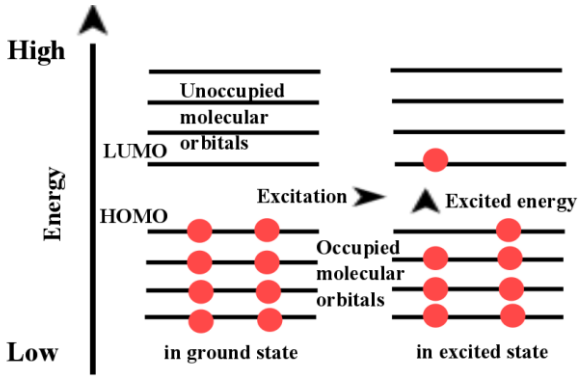

Figure 6. On the left-hand side an illustration of the HOMO and LUMO levels and on the right-hand side an electron excitation by external stimuli from the HOMO to the LUMO level.

2.6.2 Hopping Transport Model

Due to the disordered states of organic semiconductor materials and their weak intermolecular bonding, the charge transport here is localized instead of delocalized system.[9] The hopping transport model [10] can be used to show how this phenomenon happens. The mobility of the charge carriers depend on activation energy. This energy relies on the density of states distribution and tends to increase if the amount of neighboring states is large.

The charge transport mechanism in disordered organic materials is influenced by the polarization effect, which can be described by a potential well configuration in quantum mechanics. E.g. a charge is trapped in a well inside an energy barrier (a localized carrier) and only with a sufficiently large energy; this charge can overcome the small energy barrier and can move on to the next well. This can be

seen as a *hopping* mechanism as charge carrier is jumping from one site to another. At elevated temperatures, with sufficient thermal energy, it can be described as a series of charge carriers hopping between localized states from one site to another. However, at lower temperatures, charge transport happens only by tunneling.

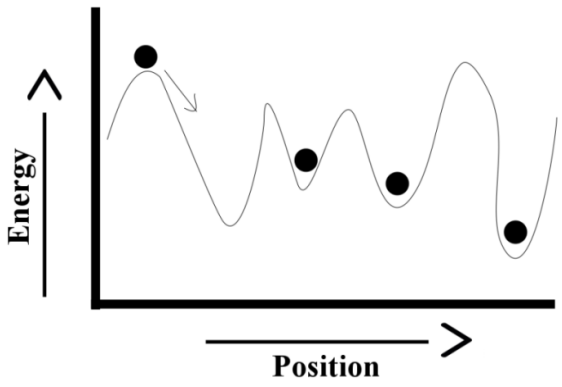

Figure 7. Hopping transport of electrons between localized states.

2.6.3 Variable Range Hopping Transport

In the hopping model charge transport is governed by the thermally activated tunneling of charge carriers in between localized sites. The concept of variable range hopping transport differs from this pattern and describes the charge transport as follows. A charge carrier variably either hops over a smaller distance with high activation energy or over a longer distance with relatively low activation energy.

In an OFET, an applied gate bias voltage increases the carrier accumulation near the semiconductor-insulator interface. As these carriers in the accumulation layer gradually fill the lower energy states of the semiconductor, excess carriers in this layer will require less activation energy to hop to a neighboring site. The effective mobility of these carriers can be expressed as [11]:

$$\mu'_{n} = \alpha\,(-Q'_{C})^{\beta} \qquad (2.7)$$

Where α is an effective overlap parameter which influences the tunneling between two localized states and for moderate and strong accumulation β can be expressed as:

$$\beta = 2\left[\left(\frac{T_o}{T}\right) - 1\right] \qquad (2.8)$$

Where T_o is the effective temperature. These equations are modified form of the traditional MOSFET equations.

2.7 Floating-gate Sensing Platform

To construct the charge based detection platform using floating-gate OFET, I have used bottom-gate, top-contact, Al-OFET structure with anodized Al_2O_3 dielectric with a silane group SAM and highly conductive P3HT as semiconductor. PET was used as substrate and glass was used just as substrate holder.

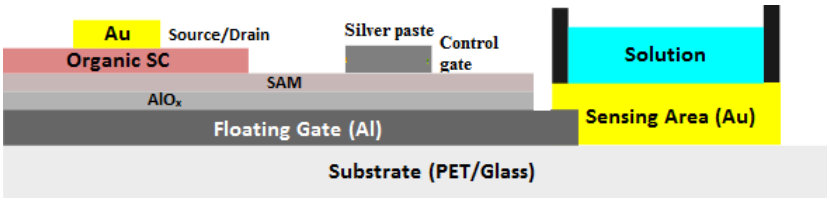

Figure 8. A schematic diagram of an OFET sensor, with the different functionalizable layers.

2.7.1 The Substrate

The deposition of a metal on a plastic substrate, e.g. PET, by vacuum evaporation, is the most commonly used technique in TFT production. The adhesion between metal and PET depends on mechanical and chemical bonds at the interface. When metal is heated and evaporated, the metal atoms collide with the PET surface and lose some energy in this process. Condensation takes place and metal atoms start forming a continuous metallic layer on the substrate. This interaction is dependent on how the substrate morphology reacts with the metal atoms. The PET film surface consists of carbonyl, hydroxyl, and vinyl groups. The surface energy of PET depends on these groups and they can create chemical reactions with the metal atoms, in a reaction called *chelation.*[12] The mechanical bond is dependent on how deep the metal atoms can penetrate the PET surface and react with the amorphous areas. The amorphous areas of the PET surface help the metal atoms to drill into the structure. The energy released upon the condensation of the metal atoms melts the surface and forms anchors to the surface crystals.[12] By these interactions, a metallic layer is formed upon the PET substrate, which is on nanometer scale. This process can be contaminated in various ways. For instance, residual metals left in the evaporation chamber, dust on the PET substrate or

water molecules might change the surface morphology and result in a metallic layer with faults. Care should be taken in order to minimize these effects.

2.7.2 The Gate Electrode

Aluminum is one of the most abundant elements on earth. It is used in various conventional micro-electronics technologies. Also, in the fabrication of TFTs for solar cells and in other thin film devices, Al is widely used as a building block.[13] With low density and sheet resistance, excellent conductivity and good ability to resist corrosion, Al is a suitable choice of material for the gate electrode. There are several physical vapor deposition (PVD) techniques to make the desired gate structures e.g. on PET substrates. Thermal evaporation is one of the most commonly used. Al has a melting point of 660°C, which makes thermal evaporation is easy and good enough for surface deposition. It is also the most simple and cost-effective technique for large scale surface deposition of metal electrodes. By using a vacuum chamber evaporation process and a specific shadow mask, the desired structure can be achieved. The evaporation of Al on silicon wafer and glass is extensively used in solar cell production.[14] Bendable substrates, e.g. polyethylene terephthalate (PET) films are relatively new. With its flexibility, good temperature resistance and low cost, PET is an excellent choice of substrate for Al deposition. It's also easy to work with, which makes it a suitable substrate for pattern design.

2.7.3 The Gate Dielectric Layer

With the increase of the metal atomic number, the ionic radius increases. But in metal oxides, the cohesive force decreases, which results in a larger dielectric constant, namely high-*k* materials.[15] A thinner dielectric layer gives the possibility for low-voltage applications and also enables the chance of higher drive voltage which allows the transistor to switch faster. Al_2O_3 has a *k* value~10,[16] which is not better than the other dielectrics used in conventional inorganic MOS technologies but aluminum oxide goes best with the aluminum gate in this case because the oxide is grown inside the aluminum by transforming the aluminum surface by chemical anodization.

As stated above, using a high-*k* gate insulator it is possible to prepare devices operating at low voltages.[1718] A common technique used in order to achieve this is to use an ultra-thin dielectric layer, consisting of a metal-oxide layer and a self-assembled monolayer (SAM).[19] By electrochemical oxidation of the gate metal, an ultra-thin, pinhole free and highly capacitive gate insulator can be formed.[20]

2.7.4 The Self-Assembled Monolayer

'SAMs are ordered molecular assemblies formed by the absorption of an active surfactant on a solid surface'.[21] A SAM treated metal oxide, used as a dielectric layer, has been shown to result in better performing devices.[222324] As the characteristics of the conjugated polymer used in the transistor is highly dependent on the surface morphology and the orientation of the crystal formation, it is important to take necessary steps in order to ensure that the surface the

polymer is applied to is both morphologically and potentially homogeneous. The semiconductor-dielectric interface layer is the most important part of the TFT. In a bottom-gated architecture, current travels within few nanometers of the gate dielectric.[25] The morphology of the polymer controls most of the charge transport characteristic of the whole TFT.

The ordering of the polymer semiconductor in its crystal structure, affects the characteristics and the mobility of the TFTs on a large scale and it is important to improve the ordering on a nanoscale level. Inserting an interfacial buffer layer e.g. a SAM in order to improve the device performance is common practice. One of the main reasons being that is easily and robustly solution processable.[26] The spontaneous formation of a 2-D system (the SAM) on a solid surface is a result of chemical reactions attaching one end of e.g. a silane to a gold atom,[26] all over the dielectric surface. This easy and fast fabrication technique makes SAMs an attractive component for surface modification and engineering. In 1997, Jackson and his colleagues reported a dramatic improvement in OFET performance using octadecyltrichlorosilane (ODTS)-treated SiO2 as a gate dielectric.[27] The dielectric surface properties determine the molecular and chemical ordering of the semiconductor, during the deposition process. SAM treated metal-oxide layer showed better orientation of the semiconductor polymer so it's a suitable technique to improve the performance of the OFET.[28] It is also shown that by using mixed SAM better control over turn on voltage in low-voltage OFETs can be achieved and octadecyltrichlorosilane (ODTS)-treated Al_2O_3 dielectric layer showed a good performance.[22]

2.7.5 The Semiconductor Layer

Polythiophenes are a class of polymers which are extensively used and investigated as the semiconductor layer in various organic devices. In particular, poly(3-hexylthiophene) (P3HT), is the most prominent candidate in this family. The optoelectronics and properties of P3Ht devices have been used and tested in numerous studies up to date.[2930] Because of the well-defined molecular architecture of this regio-regular polythiophene, there is a strong tendency for highly ordered morphology and crystallinity during fabrication. The strong intermolecular interaction is, however, the main reason for the highly efficient charge transport characteristic.[3031] The solvent used to prepare the P3HT solution and the deposition technique used to prepare the thin film, plays a crucial role in device performance. Thin film fabrication can be made cheap and fast and result in high quality homogeneous films. Drop coating, spin coating etc. are few popular deposition techniques used to prepare the different layers of an OFET. In these processes, the crystallization of the polymer takes place during drying of the film.

It has been shown that spin coating the semiconductor, using a high boiling point solvent, e.g. 1,2,4-trichlorobenzene (TCB), it is possible to improve the charge mobility characteristic of the P3HT transistors.[3230] As a direct result of the solution deposition technique, two particular and different film formations have been reported for P3HT films, i.e. edge-on and face-on. In the edge-on texture, the π-stacking of the polymer chain is in the plane of the film and the side chains point along the normal of the substrate. The fast charge transport happens along the π-stacking direction of the polymer chain; therefore the edge-on polymer formation is more desirable in OFETs. [3334] It has been shown that during the

semiconductor film forming process, a slower evaporation rate of the solvent, tend to form higher percentage of edge-on orientated polymers. [3530] Also a substrate pre-treated with a SAM improves the chance of edge-on orientation in the crystal formation process of P3HT.[28] Conventional deposition techniques e.g. spin-coating, gives highly randomly orientated polymers due to the non-equilibrium conditions. Therefore, controlling the spin coating process by aforementioned techniques, gives better orientation in the crystal formation process and thus improves the device performance.[35]

2.7.6 Bottom-Gate Top-Contact Structure

In my work, using a bottom-gate top-contact structure is helpful, due to the geometrical properties of such devices. Something called a floating gate transistor structure was used. Here, the floating gate is actually the ordinary transistor gate, modified to be used as a sensor and a second; control, gate is added to apply the gate voltages to. Using a metal electrode as the surface of the actual sensing part makes it compatible with aqueous media. Also, the dielectric surface is fine-tuned by using a SAM, in order to improve the surface morphology of the semiconductor. The surface energy of the SAM used is closer to that of P3HT compared to that of aluminum oxide. That is why the addition of the SAM also improves the adhesion of the semiconductor on top of the dielectric layer.

2.7.7 Floating Gate

The transistor is used as a sensing device for biological analytes. The main structure of the device, which consists of the transistor part, is being electrically isolated from the sensing part, because of the biological analytes being tested are located in an aqueous medium. It is hard to maintain a proper functioning OFET in an aqueous medium, due to oxidation and surface degradation of the organic semiconductor. Therefore, an extended part of the bottom-gate, which can be controlled by electrical voltage from a control point, can be used as a preferred structural design which is shown in fig. 8. The extended Al gate is connected to the sensing part of the device. When charges are placed on the sensing platform it will change the total amount of charge on the floating gate, changing the transistor electrical characteristics. This type of design is known as a floating gate-design, due to the control gate is isolated by a capacitance from the main device structure. The floating gate does not act independently in any fashion. It senses the detectable charges on the sensor metal surface and becomes charged. The excess charge should then be detected as a threshold voltage shift, when measuring the transfer curves. The extension of the gate structure adds flexibility in the design. As the main transistor part is fully isolated from the sensing part, the aqueous media in the analyte will not be able to degrade the transistor and reproducibility can be ensured. Inorganic floating-gate transistors are used to fabricate non-volatile analogue storage. This design can, however, also be useful in OFETs in biosensor applications, where charge based sensing are performed as the main operation. Floating-gate OFETs have already been reported in various studies.[3637]

2.7.8 Model Description of the Platform

The charge based detection platform can be divided into two parts: i) the transistor and ii) the sensing platform. The sensing platform is isolated from the main transistor part and is connected via the floating gate. Biological analytes should be deposited on the sensor part and the change in charge on the floating gate can be measured by the transistor part. The main gate voltage is controlled by a control gate separated from the floating gate by the gate dielectric. The difference in charge can be measured as a threshold voltage shift in the transistor transfer curve. The sensing area will be remaining enclosed by an O-ring or another isolation technique, in order to prevent spreading of the liquid buffer solution. Multiple measurements can be performed using the same OFET. Further modification of this design can add more sensing areas with a single OFET in its heart. The OFET threshold voltage shift can be measured, defined by the equation $\Delta Vth = Q/C_{TOT}$, (where Q is the immobilized charge and C_{TOT} is the sum of all capacitances in the structure, including the control capacitance and the parasitic capacitances (mainly overlap capacitances between source- and drain contacts and the floating gate in the OFET.

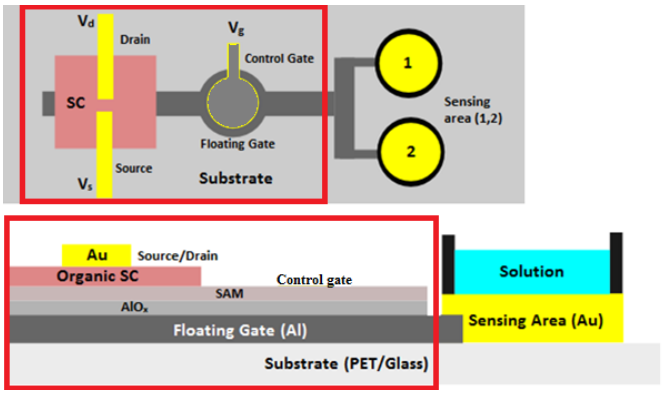

Figure 9. Schematic representation of the OFET design and the transistor part.

2.7.9 Charge Based Detection on Sensing Platform

Depending on the protein selection specific charged peptide (short chains of amino acid monomers) strands will be anchored in the Au sensing electrodes. The complementary peptide strands will be in the buffer solution to detect protein chains to attach with. If the specific protein chain is available in the solution the complementary strands will bind with those chains and as a result of these bindings the pre-deposited charged peptides will not be neutralized. If there is no protein chain to attach with these complementary peptides will bind with pre-deposited peptides and will neutralize the charge and this potential variation of the sensing electrodes will be measured by the sensor as electrical signal variation generally as a threshold voltage shift or an increase in drain current.

To mimic this biochemical reaction, often referred to as a PPTM, a less complex and less expensive method was used in this work. The sensing platform was treated with a particular type of SAM. And this SAM surface over the sensing

platform was repeatedly being charged or discharged respectively by a high and low pH buffer solution. The consecutive variation in the electrical signal (threshold voltage shift, ΔV_T) was then measured and analyzed from the adjoining OFET's transfer curve.

2.7.10 I-V Plots and Measurements

A wide range of transistor properties can be calculated using the data gathered when measuring a transfer curve, e.g. switching properties, mobility, On/Off-ratio etc. Also by analyzing the threshold voltage shift, ΔV_T, the variation in the electrical signal due to the deposited charge in the sensing platform can also be quantified.

Entities	**Definition**	**From transfer curve**
Drain On-current (I_{ON})	The measured value of the current flowing through the source-drain channel when the OFET is in on-state.	Highest corresponding point on the I_D-V_G-curve.
Drain Off-current (I_{OFF})	The measured value of the current flowing through the source-drain channel when the OFET is in off-state.	The current at the first voltage on the I_D-V_G-curve, where I_D starts to increase exponentially as a function of V_G.
On/Off-ratio (ON/OFF)	The current ratio of the OFET on-state to off-state.	Mathematically calculated as I_{ON}/I_{OFF}.

Gate Current (I_G)	The measured value of the current that flows through the gate channel when the OFET is in on-state.	The highest current on the I_G-V_G-curve.
Turn-on voltage (V_o)	The minimum value of $\|V_G\|$ above which current in the channel begins to increase exponentially as a function of $\|V_G\|$.	The first voltage on the I_D-V_G-curve where I_D starts to increase exponentially as a function of V_G.
Threshold voltage (V_T)	A gate voltage, at which I_G theoretically starts to increase logarithmically as a function of V_G.	The voltage, at which a straight line drawn on the $I_D^{1/2}$-V_G-curve, intersects with the V_G axis.
Field-Effect Mobility (μ_{FE})	The speed of the charges, in the transistor channel, during operation.	Mathematically calculated as, $\mu_{FE} = (2L/WC)[I_D/(V_G-V_T)^2]$, where L, W and C stand for the channel length, width and the capacitance of the dielectric layer.
Subthreshold slope (S)	The sharpness of the transition from off-state to on-state.	Mathematically calculated as

		$dV_G/dlogI_D$ in the region between V_{TH} and V_o, defined in units of volts/decade.

3. Experimental

Biological analytes and biologically derived recognition elements are only active in aqueous media. Therefore, it is necessary to explore the operation for aqueous systems, thus extending their applicability to a broader range of sensing needs. It is also a crucial decision to make whether the biological analytes will be deposited on the semiconductor surface for measurements or structures like extended metal electrodes will be used. Organic semiconductors are prone to react with aqueous medium and thus degrade over time. Also oxidation can degrade the semiconductor surface with a possibility of increasing conductivity. This can easily interfere with the biochemical reaction sensing and can give wrong results in analysis. Thus to ensure the stability of semiconductor surface in different buffer solutions and to check how they react in different pH values, tests were carried out to compare conductivity of semiconductor materials in high, mid and low pH solutions in a previous assignment.

3.1 Electrical Characterization of Different Semiconductors under Different pH Values

Plastic substrates coated with poly(3-hexylthiophene) (P3HT), Poly (3, 3‴-didodecylquaterthiophene) (PQT-12), P3HT 20% wt + Poly (lactic acid) or polylactide (PLA) **(**PLLA) 80% wt blend and Poly (3, 4-ethylenedioxythiophene) Polystyrene sulfonate PEDOT:PSS were used to test the conductivity. PET films were used as substrates and rinsed with DI water, followed by acetone and isopropanol before making the samples. Square sized films were attached on glass slides and then spin coated with P3HT, PQT-12 or P3HT 20% wt + PLLA 80% wt blend solutions at 1500 rpm for 40 seconds. Only P3HT and PQT-12 samples were heated at 100°C on a hot plate for 20 minutes. Au electrodes were vacuum evaporated on top of the films using an appropriate shadow mask. The thickness of the electrodes was ~ 40 nanometers and the channel length was ~30 µm. The length and widths were 30 µm and 1500 µm, respectively. PEDOT:PSS films were pre coated, Ag paste was used to make electrodes on them, the sample size was bigger than the other material's sample, roughly 2.5 cm in width and 1-1.5 cm in length each. The device structures have been illustrated in Fig 7. The devices were prepared under normal light condition and stored in the glovebox.

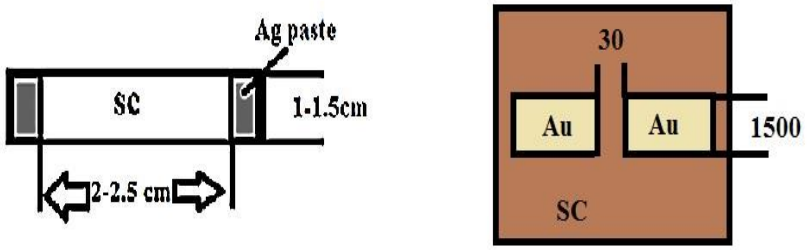

Figure 10. (Left) Sample structures of PEDOT:PSS and P3HT/PQT12/Blend samples. (Right) The channel diameters are 30 µm (length) and 1500 µm (width).

Potassium chloride (KCL), potassium hydroxide (KOH) and hydrogen chloride (HCL) were used to prepare buffer solutions. The solutions were KCl + KOH with a pH value of 11.4 (high pH value), KCl with a pH value of 5.7 and 5.8 (medium pH value) and KCl + HCl with a pH value of 2.1 (low pH value).

3.1.1 Conductivity Measurement

The conductivity between the electrodes was measured by Agilent 4142B Modular DC source/monitor measuring setup using a suitable LabVIEW program. This was done by applying a constant voltage over the two electrode pairs and measuring the current passing through the semiconductor. The conductivity was then calculated using Ohm's law:

$$V = RI \qquad (3.1)$$

Where V is the voltage applied, I is the current measured and R is then the resistance between the electrodes. The conductivity, σ, is then the reciprocal of R:

$$\sigma = \frac{1}{R} \tag{3.2}$$

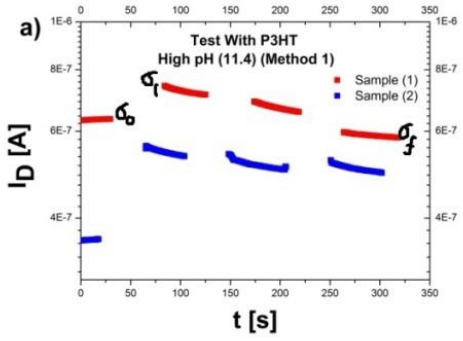

Figure 11. Example measurement to indicate how σ_o,σ_1 and σ_f are determined.

The percentage change in conductivity was measured using $\left[\frac{\sigma_f - \sigma_1}{\sigma_1}\right] \times 100\%$, ($\sigma_f$= final value, σ_1=starting value after 1st rinse) for 2nd and 3rd rinse and $\left[\frac{\sigma_1 - \sigma_o}{\sigma_o}\right] \times 100\%$, ($\sigma_o$= value just before the 1st rinse) for the 1st rinse.

Figure 12. (Left) Five pairs of source and drain electrodes evaporated onto a P3HT film. (Right) The same samples cut into stripes of individual electrode pairs. The silver paste dot was used to make the contact without damaging the Au electrodes. The PQT-12 and Blend samples were also made in a similar manner.

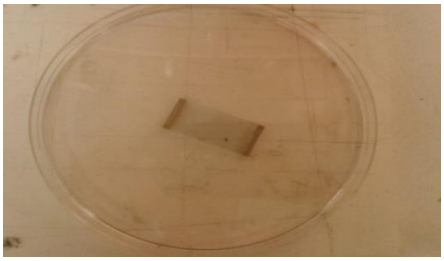

Figure 13. PEDOT:PSS stripes. Ag paste was used to make a pair of electrodes on them, the sample size was bigger than other material's sample, roughly 2.5 cm in width and 1-1.5 cm in length each.

3.1.2 Effect on conductivity of different pH value buffer solutions

All of the semiconductor materials showed change in conductivity after the deposition of buffer solution. The percentage change in conductivity was different for different pH values.

SC	Low pH	Mid pH	High pH
P3HT	18,8	9	1,9
P3HT:PLLA	9,2	8,9	16,6
PEDOT:PSS	3,4	3,6	2,1
PQT-12	7.4	25,5	19,3

Table 1. Percentage change in conductivity, calculated by " $\boldsymbol{F = \frac{\frac{Imax - Imin}{2}}{I_0} \times 100\%}$ *" of semiconductor materials under different pH value buffer solutions.*

So it can be concluded that all of the semiconductor materials had shown substantial change in conductivity measurement under different pH value buffer solutions. Biological analytes will be tested in different buffer solutions for the detection of PPTM so deposition of analytes directly over the semiconductor surface will change the actual reading due to the conductivity change of semiconductor surface itself. So a different sensor geometry which is suitable for this biochemical sensing scheme is recommended. The 'floating-gate' OFET

structure can be a good alternative for this approach and from here on I will discuss and present the works done based on floating-gate OFET sensor

3.2 Fabrication of the OFET

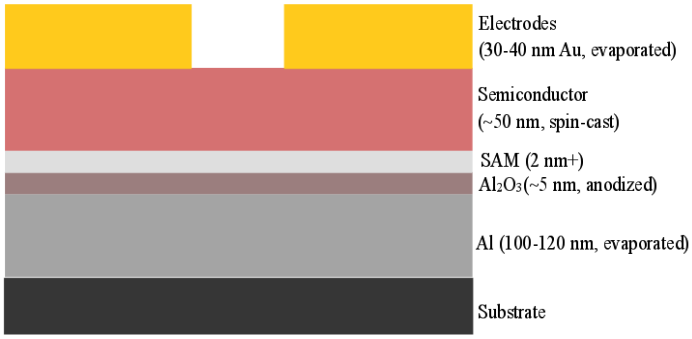

Figure 14. Schematic diagram of fabricated bottom-gate, top-contact OFET structure.

3.2.1 Substrate Preparation

A rectangular shaped PET substrate was kept in DI water and ultrasonicated for 15 minutes in 60°*C*. Afterwards it was rinsed by acetone and isopropanol. After that it was dried with nitrogen flux. Care was taken so to minimize the adhesion of dust particles and other contamination on top of the PET substrate.

3.2.2 Evaporation of Aluminum Gate

Specific patterns of 100-120 nm thick aluminum films, to be used as floating gates in OFETs, were evaporated on PET substrate. The evaporation process was done inside a vacuum chamber, inside a nitrogen-filled glove-box, at a specific evaporation rate, controlled by the current and voltage. The atmospheric pressure inside the vacuum chamber was kept at around $6*10^{-6}$ mbar, the evaporation rate was increased gradually from 0.1 $Ås^{-1}$ to 1 $Ås^{-1}$ monitored using a MAXTEC INC. model TM-100 thickness monitor. The currents and voltages were kept at 34.5-35.6A and 1.09-1.26V respectively, controlled by a Sorensen DLM 10-60 power source.

In a few cases, after evaporation, burned edges were observed in the final pattern. This may be due to faster or slower evaporation rates, increased temperatures or from metal contamination.

3.2.3 Anodization

To create a thin, pinhole free, Al_2O_3 dielectric (insulator) layer, a 100 nm thick Al gate film was chemically anodized using a citric acid- and potassium carbonate solution. The solution was prepared by diluting 0.8 gm of 28 mM potassium carbonate (K_2CO_3) in 200 ml of DI water and adding 0.528 gm of 13 mM citric acid ($C_6H_8O_7$) resulting in a citric acid anodizaion electrolyte having a pH of 6.6. The addition of the potassium carbonate only serves as a modification of the acidity of the solution. The citric acid solution has a very low pH, resulting in delamination of the aluminum films during the anodization process. An

anodization electrolyte with pH closer to 7 has been shown to result in a higher yield of working devices.

A platinum plate was used as cathode and the Al electrodes served as anodes. The voltage over the electrodes was increased gradually from 0 to 5 V, keeping the current from ever exceeding 600 μA, and the anodization, was done for no longer than 10 minutes. At the end of the anodization, a current of roughly 6 μA would circulate through the anodization circuit. When current starts flowing through the circuit, the hydrogen ions start moving to the cathode where they are reduced to hydrogen gas.

Equation of the cathode reactions:

$$2H+ + 2e- \rightarrow H_2\,(g) \qquad (3.1)$$

Simultaneously, positively charged aluminum ions (Al_3+) start to generate in the anode. At the anode surface they react with the oxide/hydroxide ions and begin to form aluminum oxide.

Equations of the anode reactions:

$$Al \rightarrow Al_3+ + 3e- \qquad (3.2)$$

$$2Al_3+ + 3O_2- \rightarrow Al_2O_3 \qquad (3.3)$$

$$2Al_3+ + 3OH- \rightarrow Al_2O_3 + 3H+ \qquad (3.4)$$

For which the overall anodization reaction of aluminum is:

$$2Al + 3H2O \rightarrow Al2O3 + 6H+ + 6e- \qquad (3.5)$$

After the anodization process the Al gates were taken out of the electrolyte and the films were rinsed with DI water to get rid of the unwanted substances and metal contamination from the substrate surface. The approximate thickness of dielectric layer is ~5 nm.

3.2.4 Drying

After the anodization and cleaning were completed the substrates were kept inside the BINDER vacuum oven in 100°*C* for at least 16 hours.

3.2.5 Plasma Treatment

Oxygen plasma treatment is a safe and environmentally friendly method for surface cleaning, activation and bonding. Critical cleaning is necessary to remove organic surface contamination from the materials thus plasma treatment is a suitable choice. By using a dry plasma treatment, the metal oxide surface can be cleaned without any mechanical damage and harmful waste. [38] It also improves the surface characteristics and the performance of the dielectric layer, by creating a more wettable gate surface. It has a significant effect on the threshold voltage. [39] The dry oxygen plasma treatment was done using a BAL-TEC/SCD050 Sputter Coater in vacuum kept at 10^{-1} mbar pressure of oxygen. A high current (6 mA) was applied over the oxygen igniting it and creating the oxygen plasma. The plasma was kept for 30 seconds in order to induce a static charge on the oxide and

in order to make a hydroxyl-rich surface, where the following SAM attachment could better adhere to the surface.[40]

3.2.6 SAM Attachment

The ODTS (Sigma-Aldrich) solution was dissolved in toluene. The solution was prepared by mixing 70 ml of toluene with 2.73 ml of ODTS. After the plasma treatment, the Al gates were submerged in the ODTS:tolune solution and kept at 60°*C* temperature for 15 minutes. After the SAM attachment the Al gates were cleaned in a n-hexane bath followed by rinse with acetone and isopropanol.

3.2.7 The Semiconductor Layer

The regioresular poly(3-hexylthiophene), OS 2100, purchased from Sigma-Aldrich (P3HT) was dissolved in anhydrous chlorobenzene (Sigma-Aldrich) (CB) at 2 wt%. The solution was heated and ultrasonicated for 30 minutes at 70°*C* and filtrated using a 0.2 μm PTFE filter. The P3HT solution was made to spin coat the OFET semiconductor layer on top of the previously attached ODTS SAM. The spin coating was done in glove box for 15 seconds at 1200 RPM. After the spin coating the samples were annealed for 20 minutes in 100°*C*.

3.2.8 The Gold Electrodes

After spin coating the semiconductor layer, the samples were kept inside the glove-box, while they were mounted into a specific shadow mask, that would create source- and drain electrodes having a channel length of 30 μm and a width of 1500 μm. Gold source- and drain electrodes were then evaporated inside the vacuum chamber.

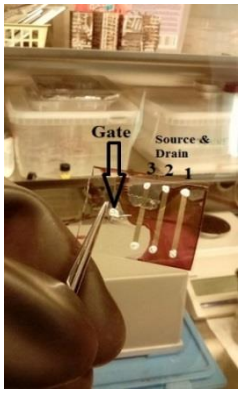

Figure 15. A PET substrate with three pairs of source- and drain electrodes, having channel lengths and widths of 30 and 1500 μm, respectively. The 100 nm thick Al gate, covered by a ~5 nm Al2O3 layer and a few nm thick SAM can be seen as a thin dark stripe across the three devices. The 50 nm thick pink semiconductor has the three Au source- and drain electrode pairs on top of it.

Under $9*10^{-6}$ mbar pressure, the evaporation rate was kept at $0.2 Å s^{-1}$ until 20nm Au had been evaporated, then for the rest of the 20nm, the rate was kept at $0.4 Å s^{-1}$. A final thickness of 40 nm was achieved for the electrodes. After the evaporation was done, silver paste was used on the edges of the electrodes in order to ensure a more robust contact, with the measurement needles, on repetitive measurements.

The circularly shaped sensing platforms were also evaporated of 30-40 nm thick Au, connected to the OFET floating gate using silver paste.

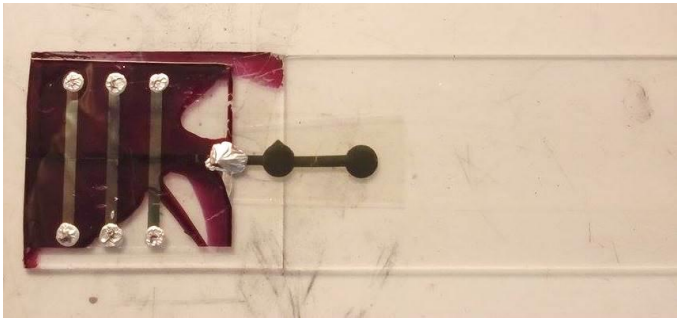

Figure 16. A picture of a completed sensor with both the transistor part (three sets of transistors all having the same floating gate) and the sensing part, joined by some silver paste.

3.3 Measurements on OFETs

All of the transfer- and output characteristics (I-V) analyses were done with an Agilent 4142B Parameter analyzer (Agilent Technologies Inc.) connected to a computer. The measurements of the OFETs were done inside a nitrogen-containing glovebox. The measuring instruments were controlled with suitable LabVIEW software (National Instruments Crop.).

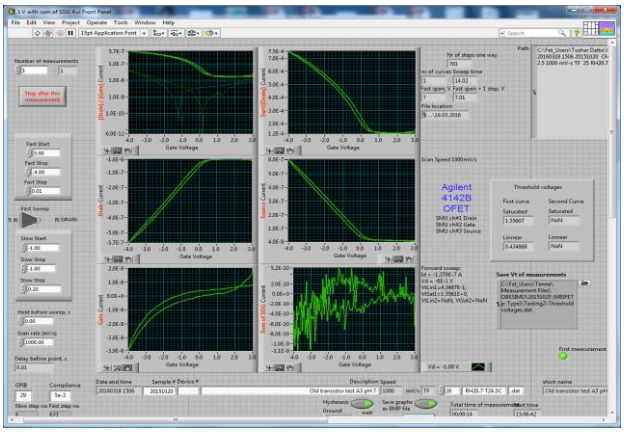

Figure 17. A screenshot of a LabVIEW program interface, used in electrical measurements.

The raw data collected with the LabVIEW programs were used to plot transistor curves using Origin software. The measurement needles were used to probe the source-, drain- and gate electrodes.

Figure 18. The measuring station with needles probing the transistor electrodes.

4. Results and Discussion

4.1 The Al_2O_3 OFET

An Al_2O_3 transistor was fabricated according to the description presented in chapter 3.2. The device was measured and stored in nitrogen-containing glovebox over a period of four months. The transistor characteristics are presented in the following sections.

4.1.1 Transfer Characteristics

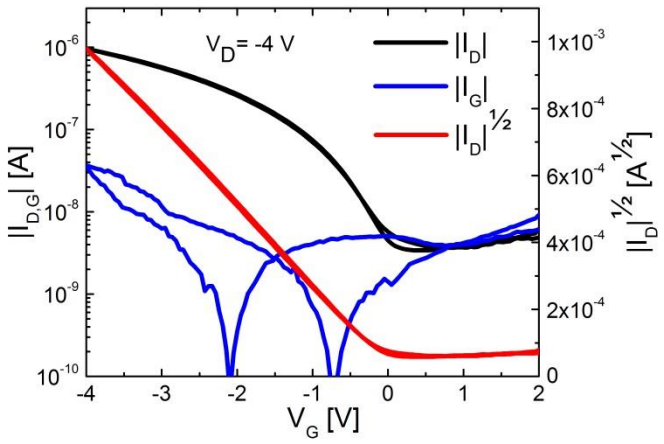

Figure 19. Transfer characteristics for a typical p-channel OFET. The transfer curve is measured in the saturated region and the square-root of I_D is also shown in the plot.

4.1.2 On/Off-Ratio

With an increasing gate potential, the OFET goes from the off-state to the on-state and I_D increases gradually. The switching behavior of the OFET can clearly be seen from the characteristic transfer curve. At higher V_G, the transistor is in on-state and shows high currents compared to those at lower $V_{G,}$ when it is in off-state. The On/Off-ratio can be obtained from the plot and mathematically, it is just the ratio of I_{ON}/I_{OFF}. In Fig. 19 it is on the order of 100. This ratio characterizes the OFET's ability to switch a signal from on to off.

4.1.3 The Threshold Voltage

In the OFET, the operating window, and by extension also the threshold voltage is heavily dependent on the thickness of the dielectric and thus is the choice of the metal oxide very important. In order to achieve high on-currents at low voltages, a thinner oxide layer is advantageous. A thinner oxide layer results in lower threshold voltages. It is a crucial improvement in the device fabrication process, which also comes with a cost. A thinner oxide layer increases the chance of higher sub-threshold leakage current, which can result in greater power consumption, or even in device failure, due to pin-holes. Also, a lower threshold voltage will result in higher off-currents. It is therefore a design trade-off. In this thesis, the design of the dielectric resulted in an oxide thickness of ~5nm and a ~2nm SAM thickness. The entire insulator layer does not extend beyond 10nm, which is fairly low. From Fig. 19, it can be seen that the threshold voltage is nearly zero, which is preferable.

4.1.4 The Turn-On Voltage

In Fig. 19 it can also be seen, that the subthreshold current starts to increase at V_G = -0.5V, which is defined as the turn-on- or onset voltage of the device. This is the minimum value of V_G, above which the conductivity between the source and the drain electrodes begins to be established and the conductivity increases exponentially with increasing value of V_G.

4.1.5 Subthreshold Conduction

The subthreshold swing, S, is defined as the inverse slope of the log (I_D) vs. V_G characteristic in the subthreshold region and can be mathematically expressed as,

$$S = \frac{d|V_G|}{d} \log|I_D| \qquad (6.1)$$

Here, the units are in volts per decade and typical values around or above S ≥ 60 mV/decade, can be found. The transition from off-state to on-state is gradual and it can be seen more clearly on a logarithmic scale. The subthreshold swing, calculated for the device, is 130 mV/decade, which is fairly good for a device having an insulator thinner than 10 nm.

4.1.6 Hysteresis

The transfer curve was swept both back and forth in order to determine if any hysteresis was present or not. Depending on microscopic effects, hysteresis can be seen in OFETs, mainly due to trapped charges in the active channel, or electrochemistry and/or slow ion movement in th electrolyte of ion-modulated transistors. A threshold voltage shift caused by a bias stress effect, can cause hysteresis in the OFET output curve.[41] From the Fig. 19, it can be seen that there is no hysteresis effect and that the OFET is performing as desired. It appears that the dielectric layer and the channel is working properly, without any substantial degradation. Also, an approximately linear slope in the liner region indicates that the contact resistance is negligible.

4.1.7 Device Parameters

The device parameters were measured and analyzed from the transistor which had the on/off ratio on the order of 100 and best performance among previously made batch of transistors and the plot is shown in Fig. 19.

Device parameter	**Value**	**Unit**
Drain off-current, I_{OFF}	$3.46*10^{-9}$	Ampere [A]
Drain on-current, I_{ON}	$9.69*10^{-7}$	Ampere [A]
Gate current, I_G	$3.73*10^{-8}$	Ampere [A]
On/Off-ratio	$2.88*10^{2}$	

Threshold voltage, V_{TH}	Nearly 0	Volt [V]
Turn on voltage, V_o	Nearly 0	Volt [V]

Table 2. The device parameters of an OFET extracted from the transfer curve plotted in Fig. 20.

4.1.8 Output Characteristics

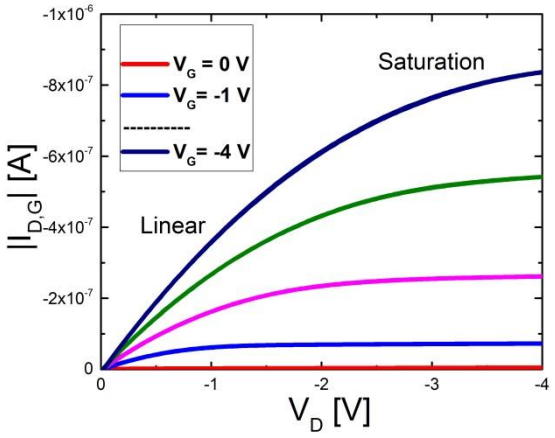

Figure 20. Output characteristics of a typical p-channel OFET.

In the output curve, shown in Fig. 20, V_D was swept at different constant V_G. It can be seen that there is a visible transition from the linear regime to the saturation regime. The device is operating in the linear regime when $|V_D| \leq |V_G - V_{TH}|$ and in the saturation regime when $|V_D| \geq |V_G - V_T|$. The linear regime lies between the threshold voltage, almost 0 V in this case and the point of pinch-off. In this region I_D increases linearly with increasing V_D.

I_D can be expressed mathematically as,

$$I_{\mathrm{D}} = \frac{W}{L}(\mu_{\mathrm{FE}}\, C_i)\left(V_{\mathrm{G}} - V_{\mathrm{T}} - \frac{V_{\mathrm{D}}}{2}\right)V_{\mathrm{D}} \qquad (6.2)$$

Where W and L are the channel width and length, respectively, and μ_{FE} is the field-effect mobility. If we assume that, $V_D << V_G$ and take the derivative of the equation with respect to V_D, the channel conductance g_D is defines as,

$$\frac{dI_{\mathrm{D}}}{dV_{\mathrm{D}}} \equiv g_{\mathrm{D}} = \frac{W}{L}(\mu_{\mathrm{FE}}\, C_i)\left(V_{\mathrm{G}} - V_T\right) \qquad (6.3)$$

This is zero in the saturated region. At, $V_D = V_G$, the charges closer to the drain becomes depleted and I_D will be pinched off because of this. Thus, the current becomes saturated. The saturated current, I_D, can be expressed mathematically as,

$$I_D = \frac{W}{2L}(\mu_{\mathrm{FE}}\, C_i)\left(V_G - V_T\right)^2 \qquad (6.4)$$

Considering that the current remains constant after the pinch-off point; $V_D = V_G$.

A different output curve of the same device that was measured in Fig. 20 has also been drawn in Fig. 21. Here, $|V_G|$ was kept below 1 V and one can see that there is much clearer saturation when the device is being measured deep in the saturated region ($V_G << V_D$).

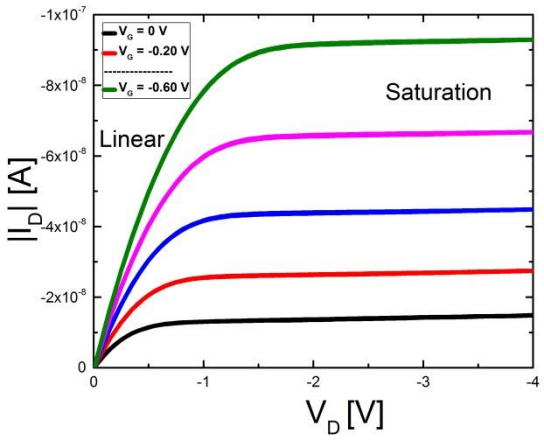

Figure 21. Output characteristics of a typical p-channel OFET measured when $V_G << V_D$.

4.1.9 Device Stability

The fabricated Al_2O_3 OFETs were kept in nitrogen-containing glovebox in minimum exposure to light. The procedure described in chapter 3.3 was followed and the same transistor device was used to analyze transfer and output characteristics after 4 months to see whether the device is stable enough to perform tests with after a long time after fabrication. The before and after transistor curves are plotted in Figs. 22 and 23. The device seems to be functioning without any substantial degradation in any of the device characteristic parameters. A slight increase in hysteresis was, however, observed. This may be due to oxidation of the semiconductor layer or due to degradation of the dielectric layer, keeping in mind that the device had been stored for four months in between the measurements.

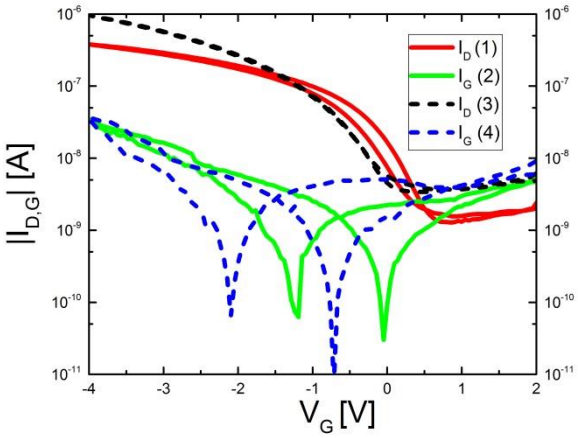

Figure 22. Transfer characteristics for a p-channel OFET. The transfer curve is measured in the saturated region. This is measured after 4 months. The dashed line plots indicate the transfer characteristic measured before 4 months.

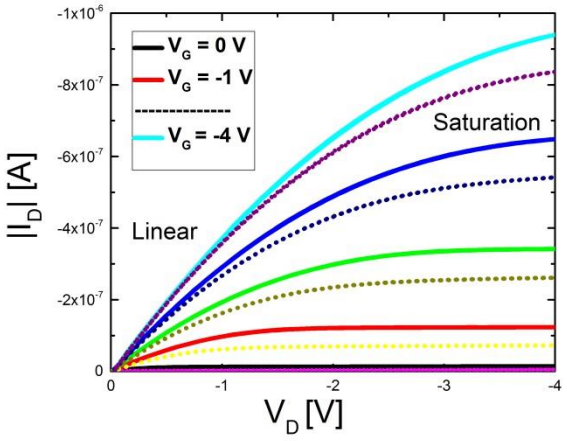

Figure 23. Output characteristics of a p-channel OFET measured after 4 months. The dashed line plots indicate the output characteristic measured before 4 months.

4.1.10 Device Parameters

The specific transistor for which device parameters were measured in chapter 4.1.7 was tested again after 4 months.

Device parameter	Value	Unit
Drain off-current, I_{OFF}	$2.03*10^{-9}$	Ampere [A]
Drain on-current, I_{ON}	$3.80*10^{-7}$	Ampere [A]
Gate Current, I_G	$3.37*10^{-8}$	Ampere [A]
On/Off-ratio	$1.87*10^{2}$	
Threshold voltage, V_{TH}	Approximately 0.5	Voltage [V]
Turn on voltage, V_o	0.53	Voltage [V]

Table 3. The device parameters of the same OFET measured after 4 months, extracted from transfer curve plotted in Fig.22.

4.2 Charge Based Detection

To mimic a biochemical reaction, often referred to as a PPTM (see chapter 2.7.9), having an electrically detectable charge, a gold surface was treated with a particular type of SAM. The SAM was dissolved in a buffer solution before its application. The SAM used was 12-mercaptododecanoic acid, MDA dissolved in ethanol, EtOH, at a concentration of 50 mM. The solution is applied on top of a gold surface and left to spontaneously assemble onto the surface. After this

process, the SAM, when placed in a high pH buffer, becomes negatively charged. After this, the charges can be rinsed away using a low pH buffer. The same process can be repeated several times. The buffer solutions used were 50 mM Na_xHgPO_4 of pH 7 and pH 2.5, respectively. Tests were carried out in two different conditions using one of the earlier made transistors, one inside the glovebox and the other outside in ambient atmosphere.

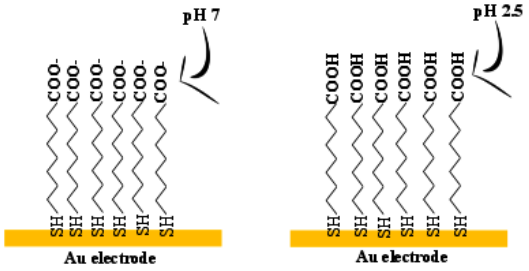

Figure 24. The activation of the SAM with a buffer solution of pH 7 and then discharging the SAM with a buffer solution of pH 2.5.

First, the sensor setup, presented in Fig. 9, was tested normally without any substance in the sensing platform. Then a droplet of MDA solution was deposited on the sensing platform. After the natural vaporization of the droplet solvent, the residue (SAM) was charged using a droplet of buffer solution of pH 7. The electrical characteristics were measured again and compared to the initial measurements and the results can be seen in Fig. 25. The buffer droplet was present on the sensing electrode surface throughout the measurement. After the measurement was done, the buffer droplet was removed and the surface was

discharged using the pH 2.5 buffer solution. The electrical characteristics were again measured.

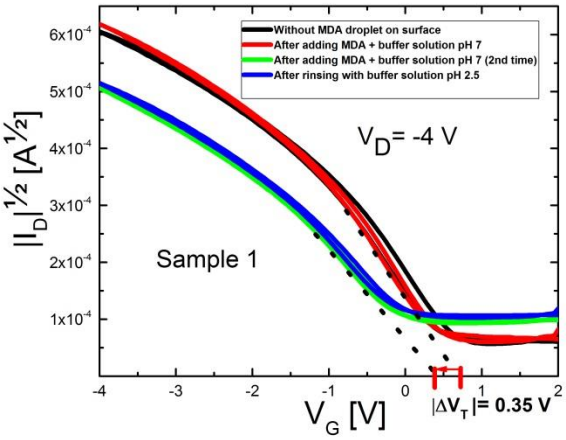

Figure 25. Electrical characteristics observed inside glove box before and after depositing MDA solution in the sensing platform.

From Fig. 25 it can be seen that there is a threshold voltage shift after the deposition of the SAM. A V_T shift, due to a charged SAM was detected. However, the shift in V_T after discharging the SAM using the pH 2.5 buffer solution was not substantial. The same sensor was then used to measure the electrical characteristics outside of the glovebox, in air. For comparison, the same measurements were repeated using another sensor. The results can be seen in Fig. 26 and 27.

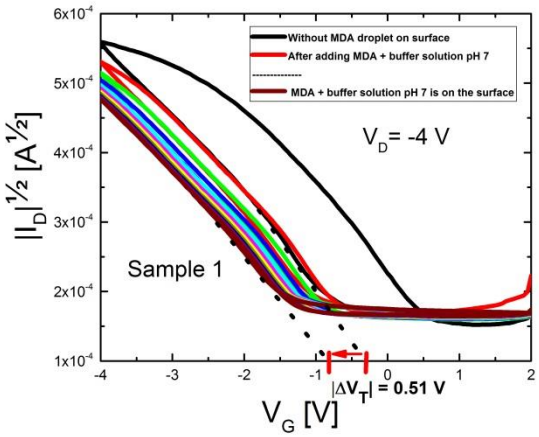

Figure 26. Electrical characteristic measurement of sensor sample 1 after the deposition of MDA solution (outside of the glovebox, in air).

This time, the sensor was measured without the MDA solution first and then the MDA solution was deposited on the sensing electrode and immediately after, charged with pH 7 buffer solution. The droplets were kept on the sensing platform and repeated measurements were done, to monitor the varying threshold voltage over time. It can be seen, that a distinct shift in threshold voltage over time, is present in this analysis. A similar shift in V_T is present also in the measurements of the second sensor, named sample 2 in Fig. 27, after the deposition of the SAM.

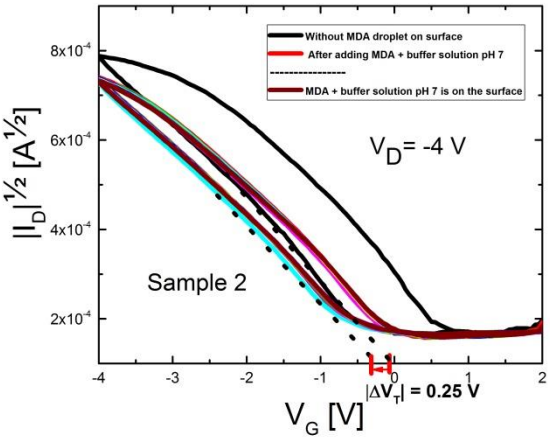

Figure 27. Electrical characteristic measurement of sensor sample 2 after the deposition of MDA solution (outside of the glovebox, in air).

It can be concluded that the sensor was able to detect some sort of variation in charge from its sensing platform, but the electrical signal change as expected, was not substantial and clear enough to be dependable. Hence, a more detailed analysis of these measurements and different methods of measurements must be done in future.

4.2.1 Bias-Stress Effect

An applied gate-source voltage, V_G can change the threshold voltage of a field effect transistor over time, which is known as the *bias-stress* effect. A negative gate-source voltage V_G in a p-channel transistor can induce this effect, which will result in shift of the threshold voltage towards more negative values. This effect is due to trapped carriers in localized states in the conduction channel or in the

dielectric. With more trapped charges over time, it can significantly change the threshold voltage towards more negative values.[42] So it is also needed to be clarified that the changes observed in these measurements are not from bias-stress effects in the OFET itself.

4.3 AFM analysis

The surface of OFETs was analyzed using atomic force microscopy (AFM), and especially the channel in between the two Au electrodes was analyzed in order to check the surface roughness and polymer growth. The AFM pictures presented in Figs. 28 and 29 have been processed using Gwyddion software. In few spots, pin holes can be seen in the channel.

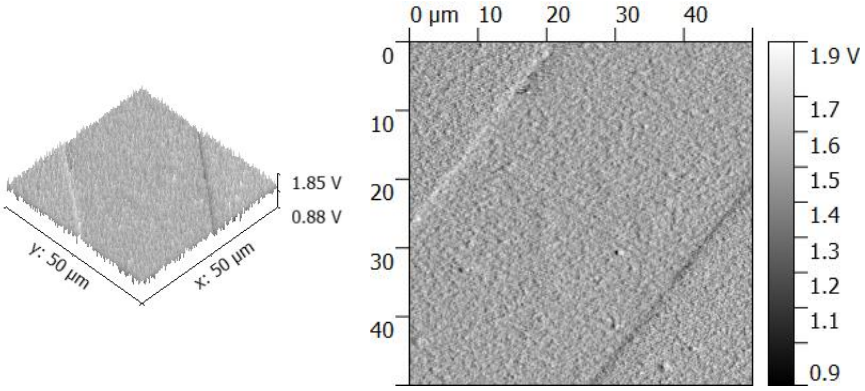

Figure 28. Surface morphology of the channel and Au electrodes over 50 µm x 50 µm surface area.

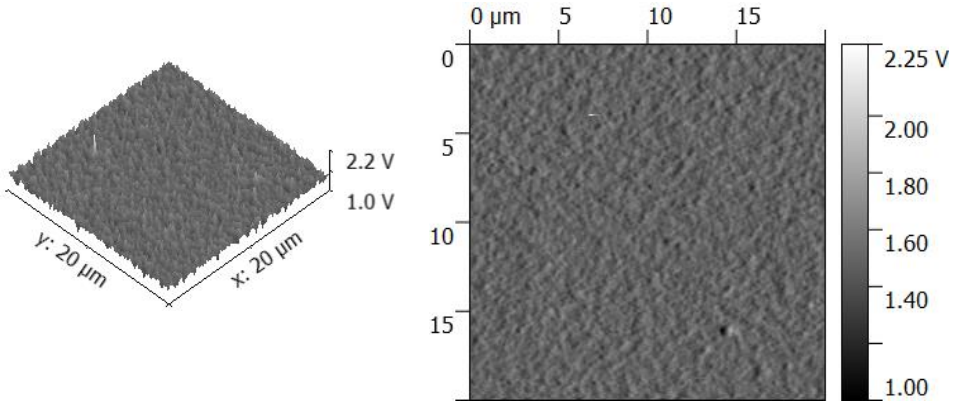

Figure 29. Surface morphology of the channel, polymer growth can be seen over 20 µm x 20 µm area .

4.4 Capacitive- and Potential-Based Detection

Because of instability of the OFET system and unclear detection of biochemical reaction from the sensing platform a different, more stable approach is proposed. The capacitive difference between two sensing electrodes will be tested using MDA solution charged with buffer solution of pH 7 and discharged afterwards with buffer solution of pH 2.5. In this setup one of the electrodes will be used as a reference electrode to compare the capacitive difference with the other electrode which is already charged with MDA solution. These two electrodes of the sensor will work as two plates of the capacitor connected with two resistors. A function generator will be used to generate square waves and an oscilloscope will be used to analyze the output waves over the capacitor connected to a computer and using a LabVIEW program. The whole setup worked as a resistor-capacitor-resistor or RCR circuit.

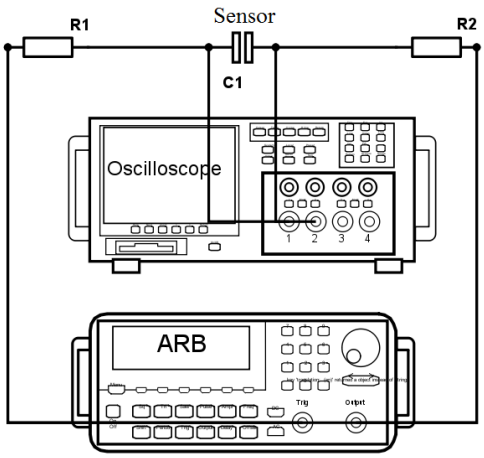

Figure 30. Simplified schematic of the RCR setup.

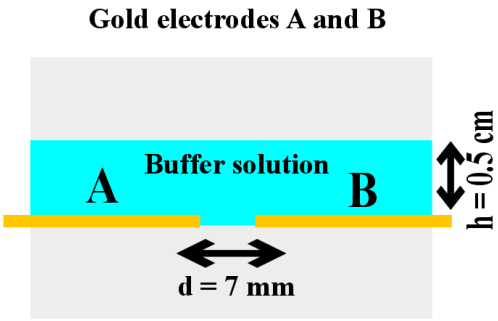

Figure 31. The structure of sensor cell.

Aforementioned procedure will also be followed and measurements will be carried out using a MISFET setup for potential based detection.

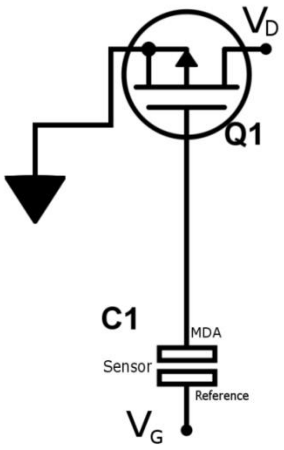

Figure 32. Simplified schematic of MOSFET setup.

The main difference in these two experiments is in the first RCR setup the capacitance change in the gold electrodes is measured directly and in the second setup the potential variation in the sensing electrodes is measured over a MOSFET via transistor transfer characteristics.

Summary

The conductivity comparison of different semiconductors under different pH values was done. The transistor part of the floating-gate OFET platform model was successfully completed and several batches of transistors were made and the quality was tested. Most of the transistors worked properly under ambient condition and showed same characteristics over four to five months without any substantial degradation. Hence, these transistors are durable, environmentally stable and reproducible in the same manner. The integration between transistor

and sensing platform was done and tests were carried out with MDA solution. The charge based detection by a threshold voltage shift was observed but more tests in different methods and thorough analysis of those data are necessary in future to clarify the outcomes. The bias-stress effect of the platform is a great concern because it can cause threshold voltage shift over prolonged measurements and can thus produce wrong results. Also the deposited charge in the sensing platform may not strong enough to actually shift the threshold voltage to a substantial amount. So the charge based detection can be very tricky and not clear enough to conclude such results. Also charge based detection platform may not be a suitable option for this kind of platform design for which a more stable approach is proposed at the end of this work.

Appendix

Chemical structures of materials used

1. **Acetone (C_3H_6O)**

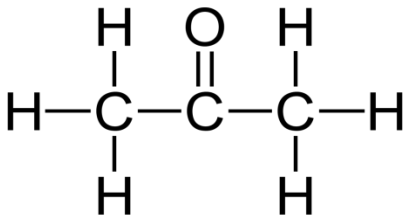

2. **Isopropanol (C_3H_8O)**

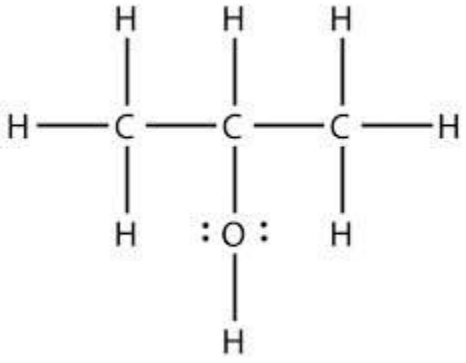

3. **ODTS ($CH_3(CH_2)_{17}SiCl_3$)**

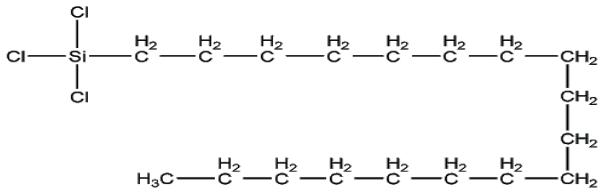

4. **1,2,4-trichlorobenzene ($C_6H_3Cl_3$)**

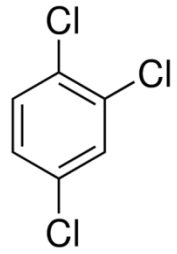

5. **P3HT ((C10H14S)n)**

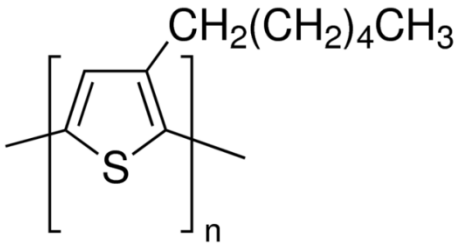

6. **Potassium carbonate (K_2CO_3)**

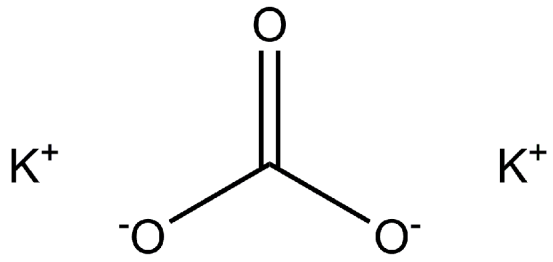

7. **Citric acid ($C_6H_8O_7$)**

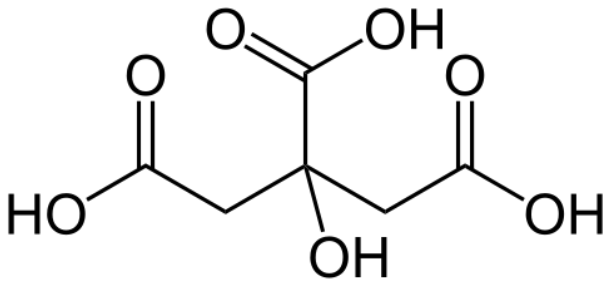

8. **PET ($(C_{10}H_8O_4)_n$)**

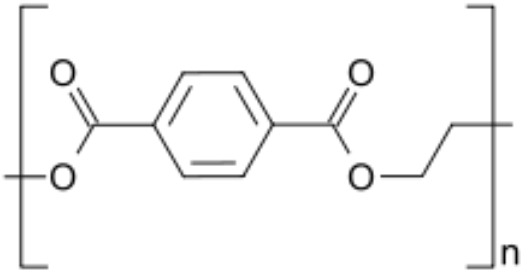

9. PLLA (Poly (lactic acid) or polylactide (PLA))

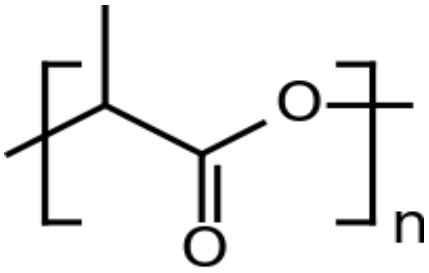

10. PQT-12 (Poly (3, 3‴-didodecylquaterthiophene))

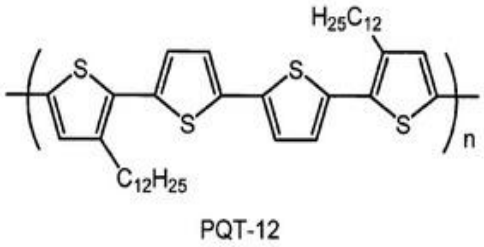

PQT-12

11. PEDOT: PSS (Poly (3, 4-ethylenedioxythiophene) Polystyrene sulfonate)

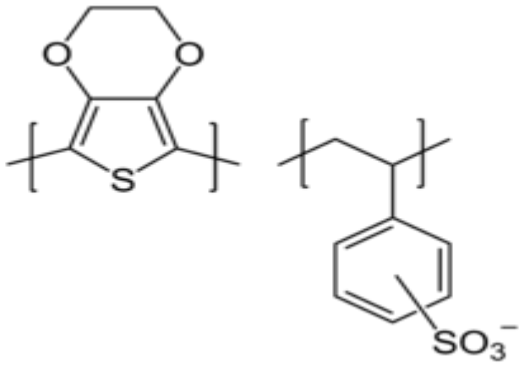

12. 12-Mercaptododecanoic acid

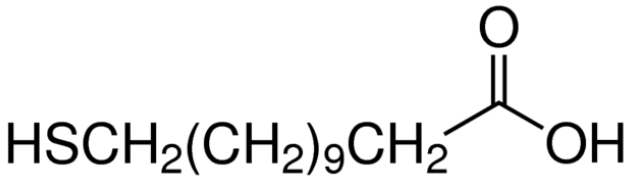

References

1. Bardeen, J. & Brattain, W. H. the_Transistor_a_Semi_Conductor_Triode. *Phys. Rev.* 1–2 (2011).

2. Kahng, D. Electric Field Controlled Semiconductor Device. US Patent 3,102,230 (1963).

3. Heeger, A., MacDiarmid, A. G. & Shirakawa, H. The Nobel Prize in chemistry, 2000: conductive polymers. *Stock. Sweden R. Swedish Acad. Sci.* 1–16 (2000).

4. Kergoat, L., Piro, B., Berggren, M., Horowitz, G. & Pham, M. C. Advances in organic transistor-based biosensors: From organic electrochemical transistors to electrolyte-gated organic field-effect transistors. *Anal. Bioanal. Chem.* **402,** 1813–1826 (2012).

5. Motorola. Field Effect Transistors in Theory and Practice. 1–12 (1993).

6. Pfattner, R., Rovira, C. & Mas-Torrent, M. Organic metal engineering for enhanced field-effect transistor performance. *Phys. Chem. Chem. Phys.* 26545–26552 (2014).

7. Gupta, D. Organic Electronics II. *Org. Electron. II* 111–117 (2007).

8. Brédas, J. L., Calbert, J. P., da Silva Filho, D. a & Cornil, J. Organic semiconductors: a theoretical characterization of the basic parameters governing charge transport. *Proc. Natl. Acad. Sci. U. S. A.* **99,** 5804–5809 (2002).

9. Fishchuk, I. I. *et al.* Analytic model of hopping transport in organic semiconductors including both energetic disorder and polaronic contributions. *AIP Conf. Proc.* **1610,** 47–52 (2014).

10. Horowitz, G. Organic electronics LECTURE 2 . Charge transport in organic semiconductors. (2014).

11. Rankov, a, Smith, E., Halls, J., Kugler, T. & Newsome, C. Modelling of organic thin film transistors for technology and circuit design Introduction to organic electronics. 11–14 (2008).

12. Culbertson, E. & Film, M. P. Metal Adhesion to PET Film. *Place Conf.* (2007).

13. Ibrahim, K. *et al.* Comparison of Aluminium Thin Film Deposited on Different Polymer Substrates With Thermal Evaporation for Solar Cell Applications. **10,** 231–235

14. Wijekoon, K. *et al.* Development of high efficiency mono-crystalline silicon solar cells: Optimization of rear local contacts formation on dielectrically passivated surfaces. *Conf. Rec. IEEE Photovolt. Spec. Conf.* 1158–1162 (2012).

15. Presented, X. SiGe grwoth model: ISSUES IN FRONT-END ENGINEERING OF CMOS NANOELECTRONICS. (2007).

16. Brezeanu, G., Brezeanu, M. & Bernea, F. High-K Dielectrics in Nano&microelectronics. *Romnet.Net* at

17. Ueno, K., Abe, S., Onoki, R. & Saiki, K. Anodization of electrolytically polished Ta surfaces for enhancement of carrier injection into organic field-

effect transistors. *J. Appl. Phys.* **98,** 1–5 (2005).

18. Misra, D., Iwai, H. & Wong, H. High-k Gate Dielectrics. *Interface* **14,** 30–34 (2005).

19. Kergoat, L. *et al.* Tuning the threshold voltage in electrolyte-gated organic field-effect transistors. (2012).

20. Majewski, L. a., Schroeder, R., Grell, M., Glarvey, P. a. & Turner, M. L. High capacitance organic field-effect transistors with modified gate insulator surface. *J. Appl. Phys.* **96,** 5781–5787 (2004).

21. Ulman, A. Formation and Structure of Self-Assembled Monolayers. *Chem. Rev.* **96,** 1533–1554 (1996).

22. Björklund, N., Pettersson, F. S., Tobjörk, D. & Österbacka, R. Controlling the turn-on-voltage in low-voltage Al2O3 organic transistors with mixed self-assembled monolayers. *Synth. Met.* **161,** 743–747 (2011).

23. DiBenedetto, S. a., Facchetti, A., Ratner, M. a. & Marks, T. J. Molecular self-assembled monolayers and multilayers for organic and unconventional inorganic thin-film transistor applications. *Adv. Mater.* **21,** 1407–1433 (2009).

24. Jalali, H. An investigation into the formation of silane-based self-assembled monolayers and the density of defects in these SAMs. (2008).

25. Tanase, C., Blom, P. W. M., de Leeuw, D. M. & Meijer, E. J. Charge carrier density dependence of the hole mobility in poly(p-phenylene vinylene). *Phys. Status Solidi* **201,** 1236–1245 (2004).

26. Lee, W. H., Cho, J. H. & Cho, K. Control of mesoscale and nanoscale ordering of organic semiconductors at the gate dielectric/semiconductor interface for organic transistors. *J. Mater. Chem.* **20,** 2549 (2010).

27. Lin, Y. Y., Gundlach, D. J., Nelson, S. F. & Jackson, T. N. Stacked pentacene layer organic thin-film transistors with improved characteristics. *IEEE Electron Device Lett.* **18,** 606–608 (1997).

28. Joseph Kline, R., McGehee, M. D. & Toney, M. F. Highly oriented crystals at the buried interface in polythiophene thin-film transistors. *Nat. Mater.* **5,** 222–228 (2006).

29. Sirringhaus, H. *et al.* Two-dimensional charge transport in self-organized, high-mobility conjugated polymers. *Nature* **401,** 685–688 (1999).

30. Bao, Z., Dodabalapur, A. & Lovinger, A. J. Soluble and processable regioregular poly (3-hexylthiophene) for thin film field-effect transistor applications with high mobility. *Appl. Phys. Lett.* **69,** 4108–4110 (1996).

31. Salleo, A. Charge transport in polymeric transistors. *Mater. Today* **10,** 38–45 (2007).

32. Chang, J. F. *et al.* Enhanced Mobility of poly(3-hexylthiophene) transistors by spin-coating from high-boiling-point solvents. *Chem. Mater.* **16,** 4772–4776 (2004).

33. Tremel, K. & Ludwigs, S. Morphology of P3HT in Thin Films in Relation to Optical and Electrical Properties. *Adv. Polym. Sci.* 1–45 (2014).

34. Aryal, M., Trivedi, K. & Hu, W. Nano-confinement induced chain alignment in ordered P3HT nanostructures defined by nanoimprint

lithography. *ACS Nano* **3,** 3085–3090 (2009).

35. Meyerhofer, D. Characteristics of resist films produced by spinning. *J. Appl. Phys.* **49,** 3993–3997 (1978).

36. Barbaro, M., Caboni, A., Cosseddu, P., Mattana, G. & Bonfiglio, A. Active devices based on organic semiconductors for wearable applications. *IEEE Trans. Inf. Technol. Biomed.* **14,** 758–66 (2010).

37. Nguyen, T. N. T., Seol, Y. G. & Lee, N. E. Organic field-effect transistor with extended indium tin oxide gate structure for selective pH sensing. *Org. Electron. physics, Mater. Appl.* **12,** 1815–1821 (2011).

38. Taylor, W. Technical Synopsis of Plasma Surface Treatments. (2009).

39. Vidor, F., Meyers, T. & Hilleringmann, U. Flexible Electronics: Integration Processes for Organic and Inorganic Semiconductor-Based Thin-Film Transistors. *Electronics* **4,** 480–506 (2015).

40. Scd, B. & Ag, B. Scientist in charge : Lhoussaine Belkoura.

41. Egginger, M., Bauer, S., Schw??diauer, R., Neugebauer, H. & Sariciftci, N. S. Current versus gate voltage hysteresis in organic field effect transistors. *Monatshefte fur Chemie* **140,** 735–750 (2009).

42. Zschieschang, U., Weitz, R. T., Kern, K. & Klauk, H. Bias stress effect in low-voltage organic thin-film transistors. *Appl. Phys. A Mater. Sci. Process.* **95,** 139–145 (2009).